https://doi.org/10.3311/PPCi.40658

Periodica Polytechnica Civil Engineering, 70(2), pp. 741–753, 2026

A Frequency-sensitive Energy-based Method for Evaluating Liquefaction Range during Vibratory Pile Driving in Saturated Sandy Soils

Huiling Zhao[1*]

[1] Department of Civil Engineering, Shanghai University, No.99 Shangda Road, 200444 Shanghai, China
[*] Corresponding author, e-mail: hlzhao@shu.edu.cn

Received: 09 April 2025, Accepted: 03 May 2026, Published online: 26 June 2026

Abstract

High-frequency vibratory pile driving in saturated non-cohesive soils can induce excess pore pressure and localized instability, posing liquefaction risks to foundation. In this study, we propose a computational framework to assess the liquefaction potential and its spatial impact range by quantifying the energy dynamics between transmitted vibration energy during pile driving and the soil's liquefaction resistance. Model-scale experiments reveal that excess pore pressure accumulation and stress redistribution occur near the pile, indicating the onset of localized instability under high-frequency excitation. The proposed method incorporates a frequency-dependent soil attenuation coefficient, $\alpha(f)$, to capture the critical role of vibration frequency in energy transmission and liquefaction behavior. The framework iteratively evaluates the liquefaction energy demand (N_{ED}) and liquefaction energy capacity (N_{EC}), enabling precise estimation of the liquefaction range. Shear modulus reduction and damping ratio curves derived from typical sandy soils are integrated into the analysis to reflect strain-dependent soil behavior. Case studies validate the method's ability to provide early liquefaction risk assessments, with practical implications for optimizing pile driving operations. Although assumptions such as neglecting pore pressure dissipation may overestimate liquefaction extent in shallow layers, the framework bridges theoretical modeling and engineering practice, offering a frequency-sensitive basis for foundation design in complex ground conditions.

Keywords

liquefaction, pile driving, vibration energy, high-frequency vibration

1 Introduction

Hydraulic vibrators with variable operating frequency and amplitude have been developed in pile driving. The geotechnical literature describes successful applications of high frequency vibrators for driving of piles, achieving high production efficiency with minimal environmental impact [1, 2]. However, careful consideration of project-specific conditions, such as the geotechnical situation, is necessary to avoid negative effects. The pile shaft is kept oscillating with a typical frequency of 20–40 Hz during vibratory driving [3, 4], in which shaft resistance is significantly low due to reduced rolling friction, liquefaction, fluidization, friction fatigue, and material degradation [5, 6]. High-frequency vibration can cause liquefaction disturbance in water-saturated granular soils. Identifying the range of liquefaction around the pile is the first step to assess the stability of piles that rely on the surrounding soil for lateral and vertical support and uneven settlement of the soil around the pile. In order to better understand the liquefaction mechanism and identify the potential for soil liquefaction, researchers have proposed different methods, which can be classified into three main groups: stress-based methods [7, 8], strain-based methods [9, 10], and energy-based methods [11]. The first two methods are better suited for analyzing liquefaction induced by earthquakes, as changes in the amplitude of the propagating motion in the soil and its response to frequency amplification and absorption need to be carefully considered. In contrast, the energy-based approach is more appropriate for analyzing liquefaction caused by vibratory driven pile vibrations with stable frequency and amplitude.

Deckner [12] and Viking [13] have discussed the transfer of energy to surrounding soil during vibratory driving. Due to material damping and wave front expansion, the vibration energy gradually attenuates with the increase of propagation distance, which is affected by the frequency and

Cite this article as: Zhao, H. "A Frequency-sensitive Energy-based Method for Evaluating Liquefaction Range during Vibratory Pile Driving in Saturated Sandy Soils", Periodica Polytechnica Civil Engineering, 70(2), pp. 741–753, 2026. https://doi.org/10.3311/PPCi.40658

material properties of the soil. Studies have been conducted to evaluate liquefaction energy capacity, i.e., the energy dissipated per unit volume required for liquefaction. This energy can be quantified as the area within the hysteresis loop developed during a loading cycle, which is dependent on the applied shear stress and shear strain. Fardad et al. [14] and Polito et al. [15] conducted stress-controlled dynamic triaxial tests and found that the energy accumulated per normalized unit volume at the onset of liquefaction does not depend on the loading shape, but rather on the loading rate. It also has been found that the dissipated energy of liquefaction of uniform sands is strongly dependent on relative density and effective stress [16, 17]. These correlations can be used to assess the liquefaction energy capacity.

Recent studies have further emphasized the importance of liquefaction assessment under different loading and ground conditions. Bán et al. [18] investigated the characterization and hazard assessment of historical liquefied sites, highlighting the importance of site-specific interpretation in liquefaction evaluation. Demir [19] examined the effects of ground-motion characteristics on the seismic response of liquefiable soils and showed that frequency content and loading duration strongly affect excess pore pressure, shear strain, and lateral response. More recently, Berrabah and Guechi [20] presented a reliability-based framework for liquefaction mitigation in stone-column-improved ground, underlining the significance of parameter uncertainty and sensitivity in engineering prediction. However, limited attention has been paid to the near-field liquefaction range induced by high-frequency vibratory pile driving, where the excitation mechanism, frequency range, and energy transfer process differ from those of earthquake loading.

The present study addresses this gap by proposing a simplified frequency-sensitive energy-based method that explicitly incorporates attenuation and strain-dependent dynamic soil properties for engineering evaluation of liquefaction extent around vibratory driven piles. In this paper, model-scale experiments first revealed significant excess pore pressure accumulation and stress redistribution near the pile, indicating the onset of localized soil instability. These observations motivated the development of an energy framework that predicts the liquefaction zone by comparing the vibration energy transmitted to the soil (N_{ED}) with the soil's liquefaction energy capacity (N_{EC}), and by evaluating whether the induced shear strain exceeds the threshold for liquefaction susceptibility. A key aspect of the method is the treatment of the frequency-dependent relationship between energy transmission and dissipation in the soil. The material damping coefficient is modeled as a function of both frequency and shear strain, which is critical for capturing the behavior of soils under high-frequency near-field vibration. The method requires only conventional geotechnical parameters typically obtained from field or laboratory tests, making it both practical and applicable for engineering design in liquefaction-prone areas.

2 Vibration driven pile model test

2.1 Test setup

A laboratory-scale vibratory pile driving model test was conducted to investigate the soil–pile interaction and pore pressure response in saturated sand. The model pile was designed as an open-ended cylindrical tube, fabricated using high-toughness resin by 3D printing. The material had an elastic modulus of 2.1 GPa and a density of 1.3 g / cm^3. The pile dimensions were 600 mm in length, 70 mm in external diameter, and 4 mm in wall thickness. The pile was driven vertically into saturated quartz sand by applying vertical harmonic excitation at a constant frequency of 33.3 Hz. The sand used in the test was uniformly graded quartz sand with particle sizes ranging from 0.5 mm to 1.5 mm. The physical properties of the sand included a specific gravity (G_s) of 2.65, a coefficient of uniformity (C_u) of 1.53, a minimum void ratio (e_{min}) of 0.514, and a maximum void ratio (e_{max}) of 0.767. To monitor the dynamic soil response during pile installation, a series of sensors were embedded within the soil mass surrounding the pile. Three accelerometers (A1–A3) were installed to capture the propagation of vibration through the soil, while five pore water pressure transducers (P1–P5) were placed at varying depths and radial distances to measure the excess pore pressure generation and dissipation induced by vibratory driving as shown in Fig.1.

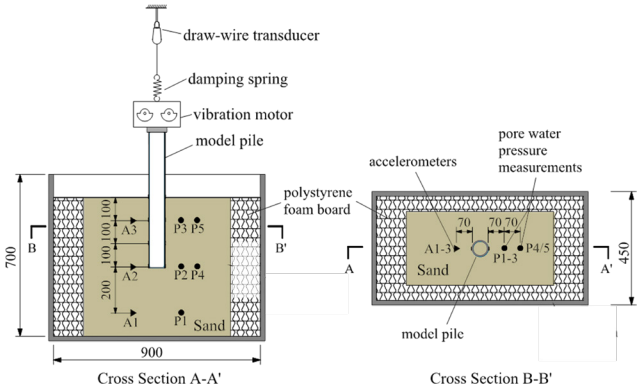

Fig. 1 Test setup of vibratory pile driving model test

2.2 Test result

2.2.1 Acceleration

The normalized amplitude spectra of acceleration in the vertical, circumferential, and radial directions as shown in Fig. 2, obtained via Fourier transform of the measured acceleration time histories, reveal distinct characteristics of the vibratory pile-soil interaction. A pronounced spectral peak is observed at approximately 33.3 Hz across all three directions, corresponding to the imposed driving frequency. This confirms the effective transmission of vibratory energy from the pile to the surrounding saturated sand. In addition to the fundamental frequency, harmonic peaks appear at integer multiples (e.g., ~16.7 Hz, ~66.6 Hz), indicating the presence of nonlinear dynamic effects and harmonic generation during pile penetration.

The vibratory energy is efficiently transmitted into the soil matrix, primarily in the vertical and radial directions. The vertical acceleration component exhibits the highest normalized amplitude, reflecting the dominant vertical energy input consistent with the direction of pile installation. The radial component also shows strong spectral responses, suggesting considerable lateral ground motion and wave propagation induced by the vibratory action. In contrast, the circumferential component displays relatively lower amplitudes, though clear spectral peaks are still present at the fundamental and harmonic frequencies. This suggests the minor asymmetries in pile geometry or soil conditions.

2.2.2 Excess pore water pressure

The excess pore water pressure responses measured by transducers P1 through P5 during vibratory pile installation demonstrate spatial variability related to both depth and radial distance from the pile. These sensors also display clear cyclic patterns corresponding to the excitation frequency of 33.3 Hz, indicating significant cyclic loading effects and the progressive generation of excess pore pressure in the active shearing zone adjacent to the pile. The excess pore pressure data (Fig. 3) show that transducers P2 and P3, located adjacent to the pile shaft, recorded the highest amplitudes, with peak values exceeding 1.0 kPa and displaying sustained cyclic fluctuations synchronized with the driving frequency. This indicates strong cyclic shearing and reduced drainage conditions near the pile, which promote the buildup of excess pore pressure and suggest a high local liquefaction potential. P4 and P5, located farther from the pile at shallow depths, showed lower values. Notably, P5 exhibited intermittent negative excess pore pressures, which can be attributed to stress relief and soil dilation caused by unloading during pile advancement.

The experimental observations presented above highlight the generation of excess pore water pressure and dynamic stress fluctuations in saturated non-cohesive soils subjected to high-frequency vibratory pile driving. The localized accumulation of pore pressure near the pile shaft, coupled with transient stress redistribution, suggests a heightened susceptibility to localized liquefaction. The test results clearly demonstrate that energy input from cyclic vertical vibrations can significantly weaken soil stability, raising critical concerns for both pile drivability and foundation performance.

Understanding the onset and spatial extent of liquefaction is essential for the safe and efficient design of foundation systems in saturated granular soils. Traditional empirical methods often fail to capture the influence of vibration frequency and energy propagation, especially under high-frequency loading conditions typical of modern vibratory pile drivers. Moreover, most existing approaches focus on point-based evaluations of pore pressure or shear strain, overlooking the broader three-dimensional influence zone where liquefaction-induced deformations may compromise

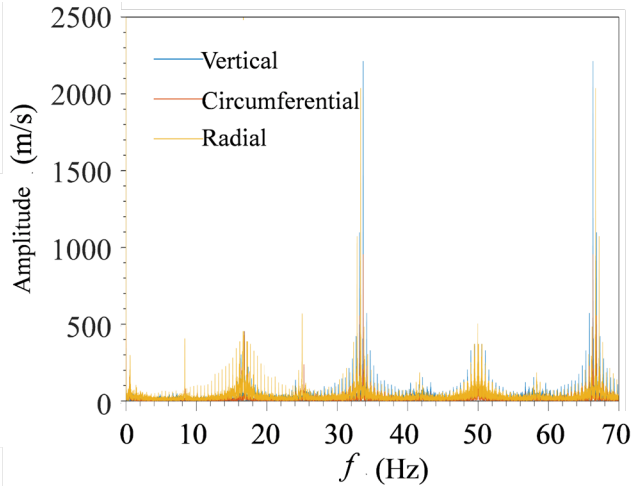

Fig. 2 Fourier acceleration spectra during vibratory pile installation

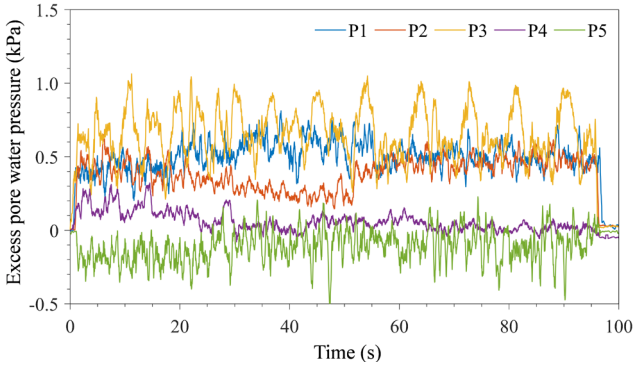

Fig. 3 Time histories of excess pore water pressure in pile installation

structural integrity. To address these limitations, a computational framework that evaluates liquefaction potential and its impact range through an energy-based approach are introduced in next section.

3 Energy-based computation model of liquefaction impact range

3.1 Characteristics of vibration driven pile in soil

To accurately evaluate the liquefaction potential and its spatial impact range during vibratory pile installation, it is essential to characterize the input conditions that govern energy transfer from the pile to the surrounding soil. The efficiency and extent of this energy transmission are largely dictated by the key characteristics of vibration-driven piles, including vibration frequency, amplitude, acceleration.

The vertical oscillation of the vibrator is produced by counter-rotating eccentric masses, generating the excitation force (centrifugal force) on the pile. The peak value of the centrifugal force, F_v, depends on the eccentric moment, M_e, and on the circular frequency, ω ($2\pi f$), of the rotating eccentric masses.

$$F_v(t) = M_e\omega^2 \sin(\omega t) \tag{1}$$

Vibrator performance is also significantly influenced by the displacement amplitude, $s_{\max}$, which relies on the eccentric moment, M_e, and the mass of the vibrating system of the vibrator, clamp and pile, m.

$$S_{\max} = M_e/m \tag{2}$$

It is important to note that the displacement amplitude, smax, is not affected by the vibration frequency, f. Vibrators equipped with variable eccentric moments offer the machine operator the ability to commence and cease vibration at zero amplitude, thereby mitigating the risk of vibration amplification resulting from resonance. Assuming that the vibration displacement varies with time as a trigonometric function with a fixed circular frequency ω, the amplitude of the vibration velocity $v_{p\max}$ can be expressed as $s_{\max}\,\omega$.

The peak value of the excitation force and the vibration displacement amplitude can significantly impact the driving efficiency and should be carefully evaluated when selecting a vibrator with a sufficiently high eccentric moment. During the process of driving with a hydraulic vibrator, the excitation force and displacement amplitude are typically controlled and adjusted based on the soil layers being penetrated. It is generally accepted that the centrifugal force is the main factor influencing vibratory pile driving in granular soils, while the displacement amplitude is a critical parameter in cohesive soils [21].

3.2 Energy transmitted to the soil

3.2.1 Energy transfer between piles and soil

Under the vertical excitation of the vibrator, the pile undergoes vertical vibration, generating compressional and shear waves that propagate outward to the soil. The vibrational energy is transmitted to the surrounding soil, causing the soil to vibrate accordingly. Holeyman [22] suggested that the failure of soil structure is mainly caused by the propagation of radial vertical polarized shear waves. Dowding [23] proposed the expression for shear strain caused by the propagation of radial shear waves as follows:

$$\gamma = v/V_s\ , \tag{3}$$

where v represents the soil particle vibrating velocity of the shear wave, while V_s represents the shear wave velocity of the soil layer, which is a function of shear strain g.

If the soil experiences significant shear strain γ, it can cause the degradation of the shear modulus G, leading to a decrease in the shear wave velocity V_s. The shear modulus ratio G / $G_{\max}$ is described as a function of shear strain, which is one of the important dynamic characteristic curves of soil. Neglecting the variation of soil density, the shear modulus is proportional to the square of the shear wave velocity. Thus the shear wave velocity V_s depends on the initial (tangent) shear modulus $G_{\max}$, the corresponding shear wave velocity $V_{s\max}$ and $G(\gamma)$. Shear strain requires iterative solution as follows:

$$\gamma = \frac{v}{V_{s\max}\sqrt{G(\gamma)/G_{\max}}}\ . \tag{4}$$

The energy associated with the rearrangement and settlement of sand particles during cyclic loading conditions is regarded as a constant quantity under specific circumstances, leading to liquefaction as observed by Figueroa et al. [16]. A typical cyclic loading test can generate the shear stress-shear strain hysteresis loop. The cumulative dissipated energy in each loading cycle is equal to the cumulative enclosed area of the hysteresis loop, which can be mathematically expressed as follows:

$$\Delta W_1 = 2\pi D(\gamma)\tau\gamma\ , \tag{5}$$

where ΔW_1 is the cumulative energy in each cycle, and D is the damping ratio of the soil.

When a pile vibrates in soil with a fixed frequency f for a time t, the unit energy transmitted to the soil around the pile N_{ED} can be expressed as follows:

$$N_{ED} = 2\pi D G_{\max}\frac{G(\gamma)}{G_{\max}}\gamma^2 \cdot f \cdot t\ . \tag{6}$$

3.2.2 Attenuation of energy during wave propagation

The presence of the interface between pile and soil causes partial reflection and complementary transmission of energy. When the vibration of a pile is transmitted to the soil, the energy transmission coefficient is less than 1 because the impedance of the pile is greater than that of the soil. The energy transmission coefficient is the ratio of transmitted energy to incident energy, i.e. T depends on the impedance of the pile z_p and the impedance of the soil z_s, as $T = 2 / (1+ z_p / z_s)$ [21].

During the propagation of waves in soil, the vibrational energy density gradually attenuates with the propagation distance. The reduction of energy density caused by the expansion of the wavefront area is termed geometric attenuation. The remaining portion of the energy is absorbed by the soil medium, also known as medium dissipation energy and termed material attenuation, which consists of the energy dissipated by particle surface friction and the viscous dissipation energy resulting from the relative movement of pore fluid to the soil skeleton.

Taking into account material damping and geometric damping, a comprehensive attenuation model [24] can be expressed as follows:

$$v_2 = v_1\left(\frac{r_1}{r_2}\right)^n \cdot \exp\left[-\alpha\left(r_1 - r_2\right)\right] \cdot T\,, \tag{7}$$

where, the parameters v_1 and v_2 represent the known and unknown amplitudes at distances r_1 and r_2 from the vibration source, respectively, while n is the geometric damping coefficient and α is the material attenuation coefficient, which is frequency-dependents.

For geometric attenuation in wave propagation, there are two commonly used calculation methods: cylindrical diffusion model (applicable to near-field regions) and spherical diffusion model (applicable to far-field regions). Herein, cylindrical model is used to calculate the vertical shear waves propagating away from the pile. Assuming the wave source is at the origin and the observation point is at a distance R from the source, the geometric attenuation depends on $1 / R$.

3.2.3 Dependence of material attenuation on frequency

Previous energy-based approaches for evaluating soil liquefaction have predominantly focused on low-frequency cyclic loading, often neglecting the frequency-dependent nature of material attenuation. However, in the context of high-frequency vibratory pile driving, this assumption may lead to significant underestimation or misrepresentation of energy dissipation in the near-field soil. The dynamic response of soil, particularly the material damping behavior, is known to be strongly influenced by both loading frequency and shear strain amplitude. Therefore, incorporating the frequency dependence of attenuation is essential for accurately modeling the energy transmission and dissipation processes in saturated sandy soils subjected to high-frequency excitation.

Table 1 presents the measured material attenuation coefficients for wave propagation at 15 Hz and 30 Hz in different soil types, illustrating the clear variation of damping characteristics with frequency. These values serve as key input parameters for the proposed energy-based liquefaction evaluation framework and highlight the necessity of site-specific frequency-dependent attenuation modeling. The data show a clear and consistent trend: material damping increases with frequency, approximately doubling in some cases. For instance, in loose sand, α increases from 0.05 at 15 Hz to 0.09 at 30 Hz, representing an 80% increase. Similar proportional increases are observed in soft clay (0.09 to 0.13) and medium dense sand (0.03 to 0.06). This trend supports the assumption that, within the frequency range relevant to vibratory pile driving (typically 10–40 Hz), the damping coefficient α can be considered approximately proportional to the excitation frequency for a given soil type.

According to the S-wave propagation theory, the material damping coefficient α is related to the quality factor Q_S and damping ratio D of the material as Eq. (8):

$$\alpha = \frac{\pi f}{Q_s V_s} = \frac{2\pi fD}{V_s} = \frac{\omega D}{V_s}\,. \tag{8}$$

The material damping coefficient α is frequency-dependent, also related to the damping ratio D and the shear wave velocity V_s, which depends on shear modulus G. The dynamic shear modulus G and damping ratio D of soil are important parameters that express the dynamic characteristics of soil. The dynamic stress-strain relationship of soil under cyclic loading exhibits nonlinearity, hysteresis, and deformation accumulation. The shear modulus G and damping ratio D of soil can be obtained through laboratory tests or in-situ tests.

Table 1 Material damping coefficient for different frequency in soil

Soil type	$V_{s\max}$ (m / s)	α (15Hz)	α (30Hz)
Soft clay	75	0.09	0.13
Loose sand	100	0.05	0.09
Medium dense sand	150	0.03	0.06
Dense sand	200	0.02	0.05
Gravel	300	0.02	0.03
Glacial till	400	0.01	0.02

As shown in Fig. 4 is G / G_{max}–γ, D–γ curves of typical sandy soil layers in Shanghai soil site.

The empirical formulas [25] of G / G_{max}~γ and D~γ are usually based on the Davidenkov model for G / G_{max} and a modified Hardin-Drnevich model [26] for D as shown in Eq. (9) and Eq. (10).

$$\frac{G}{G_{\max}} = 1 - \left[\frac{(\gamma/\gamma_r)^{2B}}{1+(\gamma/\gamma_r)^{2B}} \right]^{A} \tag{9}$$

where, A and B are fitting parameters related to soil properties, obtained by fitting experimental test data, and γ_r is the reference shear strain, with $\gamma_r = \tau_{max} / G_{max}$.

$$D = D_{\min} + D_0 \left[\frac{(\gamma/\gamma_r)^{2B}}{1+(\gamma/\gamma_r)^{2B}} \right]^{An} \tag{10}$$

where, D_{min} is the minimum damping ratio, A, B, n, and D_0 are fitting parameters related to soil properties.

Table 2 provides the fitting parameters for the G / G_{max}–γ and D–γ relationship curves for the two soil.

The relationship curve between material damping coefficient α and shear strain γ can be obtained as shown in the Fig. 5. The difference between these two sandy soil layers is

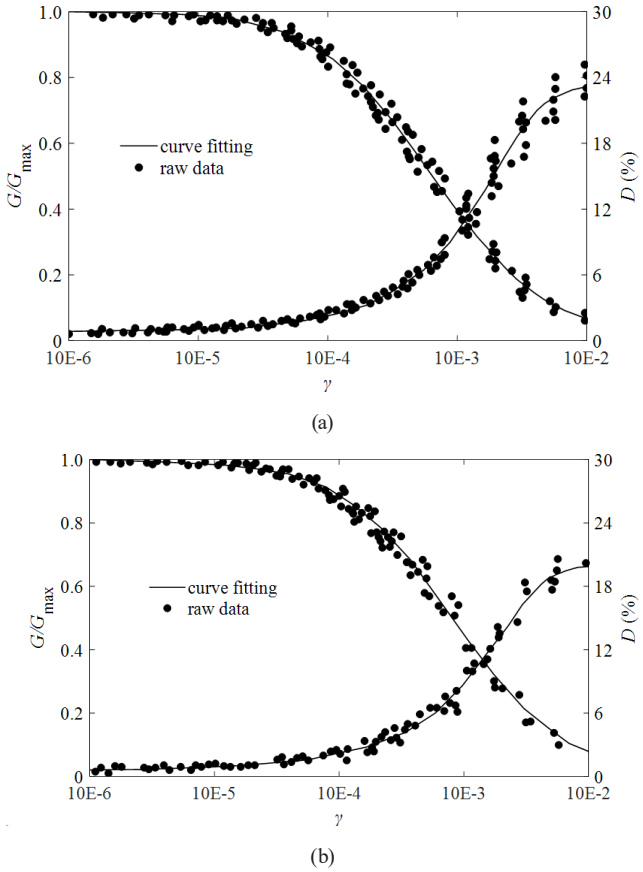

Fig. 4 G / G_{max}–γ, D–γ curves of typical sandy soil layers in Shanghai: (a) No. 3 Sandy silt; (b) No. 13 Sandy silt loam

Table 2 G / G_{max}–γ & D–γ curves fitting parameters for Shanghai sandy soil

Soil layer		Fitting parameters					
		A	B	γ (%)	D_0	D_{min}	n
No. 3 Sandy silt	G / G_{max}	1.04	0.49	0.060			
	D	0.40	1.27	0.303	22.8	0.737	0.776
No. 13 Sandy silt	G / G_{max}	1.02	0.49	0.079			
	D	0.40	1.44	0.316	19.5	0.532	0.643

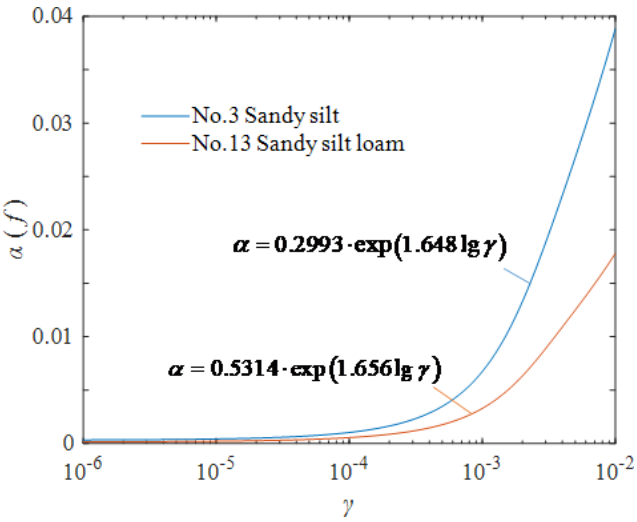

Fig. 5 α–γ curves of typical sandy soil layers in Shanghai

that No. 3 sandy silt has a larger particle size, higher permeability, and better load-bearing capacity and drainage performance. In contrast, No. 13 Sandy silt has finer sand particles, stronger water adsorption capability, leading to increased viscosity.

3.3 Capacity energy for soil liquefaction

The energy required for soil liquefaction can be calculated using the capacity energy concept. The amount of dissipated energy required for soil liquefaction is known as "capacity energy", which is closely related to several factors, including relative density, initial effective confining pressure, fine contents, and soil textural properties. The better the particle size distribution, the more stable the pore structure of the soil, the greater the compaction level and confining pressure, and the stronger the structural integrity of the soil, the higher the energy required for liquefaction. In field tests, measuring the penetration resistance of the soil is a commonly method to evaluate the capacity energy for liquefaction [27, 28].

Green [11] suggested to calculate the capacity energy NEC for soil liquefaction using the corrected standard penetration resistance as follows:

$$N_{EC} = 1.195 \exp\left(0.185 N_{1,60CS}\right). \tag{11}$$

$N_{1,60cs}$ refers to the corrected standard penetration test (SPT) blow count recommended by the National Earthquake Engineering Research Center in the United States and used to correct for the effects of fine-grained soil content on the penetration resistance measurements obtained from standard penetration tests (SPTs) and calculated as follows:

$$N_{1,60CS} = \alpha + \beta N_{1,60}\,, \tag{12}$$

where, α and β are correction coefficients based on the fine particle content F_c, and expressed are as follows:

$$\alpha = \begin{cases} 0 & F_c \\ \exp\left[1.76 - \left(190/F_c^2\right)\right] & 5\% < F_c \le 35\% \\ 5 & F_c > 35\% \end{cases},$$

$$\beta = \begin{cases} 1.0 & F_c \le 5\% \\ \left[0.99 - \left(F_c^{1.5}/1000\right)\right] & 5\% < F_c \le 35\% \\ 1.2 & F_c > 35\% \end{cases}$$

3.4 Determination of the extent of liquefied zone

This section presents a method for determining the liquefaction zone. The method is based on comparing the energy transmitted to the soil through high-frequency pile driving N_{ED} with the energy capacity for soil liquefaction N_{EC}, which is used to determine whether liquefaction occurs.

The critical conditions for liquefaction susceptibility is as follows:

$$N_{ED} = 2\pi D(\gamma) G_{\max}\left[\frac{G(\gamma)}{G_{\max}}\right]\gamma^2 \cdot ft \cdot \frac{\sigma_r'}{\sigma_m'} = N_{EC}\,. \tag{13}$$

This critical condition takes into account the lateral stress correction of the soil. The average effective confining stress is related to is vertical effective stress.

$$\sigma_m' = \frac{1+2K_0}{3}\sigma_v' \tag{14}$$

The second important condition for liquefaction is that the soil experiences shear strain exceeding a certain threshold. The shear strain threshold γ_q for liquefaction susceptibility is the minimum shear strain value at which soil begins to liquefy. Different researchers have proposed different values for this threshold, depending on the soil type and history. Gujrati [29] found that the shear strain threshold for triggering pore water pressure buildup and liquefaction of sand is 0.017% by the cyclic strain method. According to Kishida's field study [30] that analyzed the data from 13 earthquake events and sugessted the shear strain threshold for liquefaction susceptibility 0.015%. In this article, the shear strain threshold γ_q is chosen as 0.015%, which is suitable for sandy soil.

If the energy transmitted to the soil exceeds the energy capacity for liquefaction, and causes shear strain in the soil to exceed the threshold γ_q at a specific location, then it is likely that liquefaction has occurred. By repeating this process at multiple locations, it is possible to delineate the extent of the liquefied zone. The shear strain induced in soil by vibratory pile driving attenuates gradually with increasing distance from the pile. If the pile is vibrated for a long time in a certain layer of soil, the vibration can propagate far, resulting in a larger area of shear strain that gradually decreases until reaching the shear strain threshold γ_q, within which is the liquefaction zone. However, if the pile is vibrated for a short duration in a certain soil layer, the shear strain may not attenuate to the shear strain threshold γ_q, resulting in a smaller liquefaction zone. We can use the liquefaction critical condition $N_{ED} = N_{EC}$ at the point with shear strain γ_q to provide a time threshold t_q for evaluating the duration of vibration. It should be noted that this method does not consider the drainage during the vibration, which may overestimate the liquefied zone of shallow soil. It is limited to determinate the range of near-field liquefied zone in the sandy soil.

The specific steps for determination of the extent of liquefied zone are as follows:

1. Test the dynamic properties of soil. Conduct a series of cyclic triaxial tests on soil samples to determine $G_{\max}$, and calculate the G / $G_{\max}$–γ, D–γ relationships to evaluate V_s–γ, and α–γ.
2. Obtain the characteristic parameters of the pile-driving vibrator. Calculate the amplitude of the vibratory force, F_v, and the amplitude of the vibration displacement, $s_{\max}$. Based on the vibration frequency f, calculate the amplitude of the vibration velocity $v_{p\max}$.
3. Calculate the transmission coefficient T by the interface between the pile and the soil depends on the impedance of the pile z_p and the impedance of the soil z_s. The amplitude of the soil particle's vibration velocity at $r = 0$ around the pile, $v_{\max}$, can be calculated.
4. Acquire the pile driving velocity. The vibration duration (t) in a soil layer can be calculated from the pile driving velocity.
5. The liquefaction area of non-cohesive soil induced by pile driving vibration can be obtained through the flowchart below, as illustrated in Fig. 6.

To improve clarity and reproducibility, the main symbols, thresholds, and units used in the proposed method are summarized in Table 3.

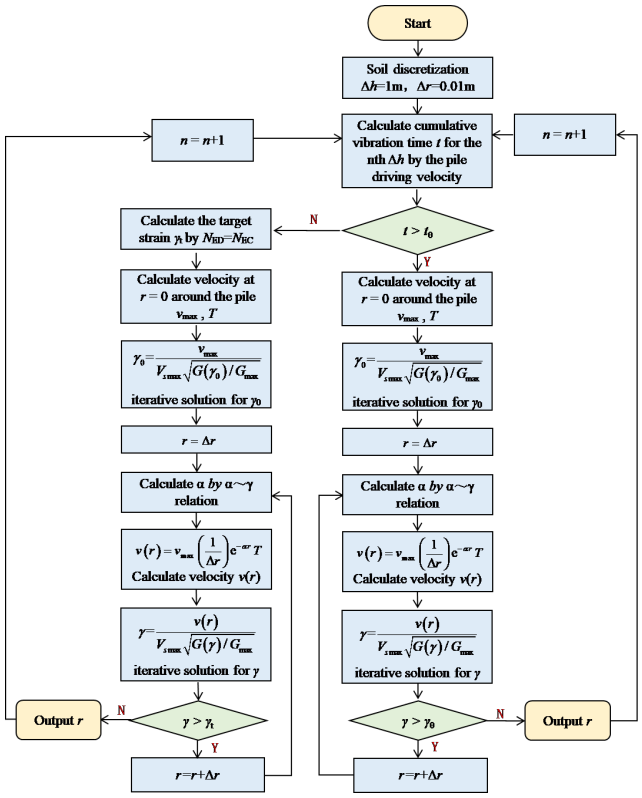

Fig. 6 Liquefaction zone determination flowchart

4 Case study and validation

To assess the applicability and predictive capability of the proposed energy-based model under real-world conditions, two field case studies were selected for validation. These cases involve high-frequency vibration in saturated sandy soils, where detailed pore pressure and acceleration measurements were available. By applying the developed framework to these practical scenarios, the model's performance in estimating the liquefaction impact range can be evaluated against observed in situ responses, thereby demonstrating its relevance for engineering applications.

4.1 Case 1

Zhan et al. [31] and Wei [32] conducted a series of field test of high-frequency driving piles in a soil site in Shanghai. The steel pipe piles were 22 m in length, with a diameter of 0.7 m. The pile toe was situated at a depth of 53 m below the ground. One of the soil layers at this site is No. 3 sandy silt layer with 10 of N blows from SPT (at a burial depth ranging from 2.4 to 4.9 m and below the water table). The vibratory driving force used for pile driving in this layer is 1400 kN and with vibration frequency 33.3Hz.

The vibratory driving force and the number of blows N from SPT prior to pile driving are also displayed in Fig.7.

Table 3 Summary of key symbols, thresholds, and units used in the proposed method

Symbol	Meaning	Unit	Note / criterion
f	Vibration frequency	Hz	Typically 10–40 Hz in vibratory driving
F_v	Excitation force amplitude	kN	Determined by vibrator properties
$s_{\max}$	Displacement amplitude	m	From eccentric moment and vibrating mass
$v_{p\max}$	Pile vibration velocity amplitude	m/s	$v_{p\max} = s_{\max}\,\omega$
$v_{\max}$	Soil particle velocity amplitude near pile	m/s	Includes transmission effect
T	Energy transmission coefficient	–	Pile–soil impedance dependent
G / $G_{\max}$	Modulus reduction ratio	–	Strain-dependent
D	Damping ratio	–	Strain-dependent
α	Material attenuation coefficient	1/m	Frequency- and strain-dependent
γ	Shear strain	%	
γ_q	Shear strain threshold	%	Adopted as 0.015%
N_{ED}	Liquefaction energy demand	J / m^3	Computed from vibration loading
N_{EC}	Liquefaction energy capacity	J / m^3	Estimated from SPT-based correlation
$N_{1,60CS}$	Corrected SPT blow count	–	Includes fines correction
σ'_m	Average effective confining stress	kPa	Used in liquefaction criterion
η_d	Dissipation reduction factor	–	Optional factor for shallow drainage correction

The excess pore water pressure ratio around the pile during the pile driving process was measured during this soil layer. The α–γ relationship based on the G / $G_{\max}$–γ and D–γ relations is employed as shown in Fig. 4.

According to Section 3, the extent of liquefied zone was determined to compare with the test results. Experiments and field observations [33, 34] also have found that the sandy soil often liquefies when the excess pore pressure between 0.6 and 0.7. In the test, an excess pore water pressure ratio of 0.7 was taken as the liquefaction criterion. Fig. 8 presents contour plots of excess pore water pressure ratios obtained from on-site tests with value of 0.7 as well as the liquefaction range obtained by the calculation.

The liquefaction range calculated in this paper was found to be larger than the on-site measured results, which may be mainly attributed to the rapid dissipation of excess pore water pressure during the pile driving process in the shallow sand

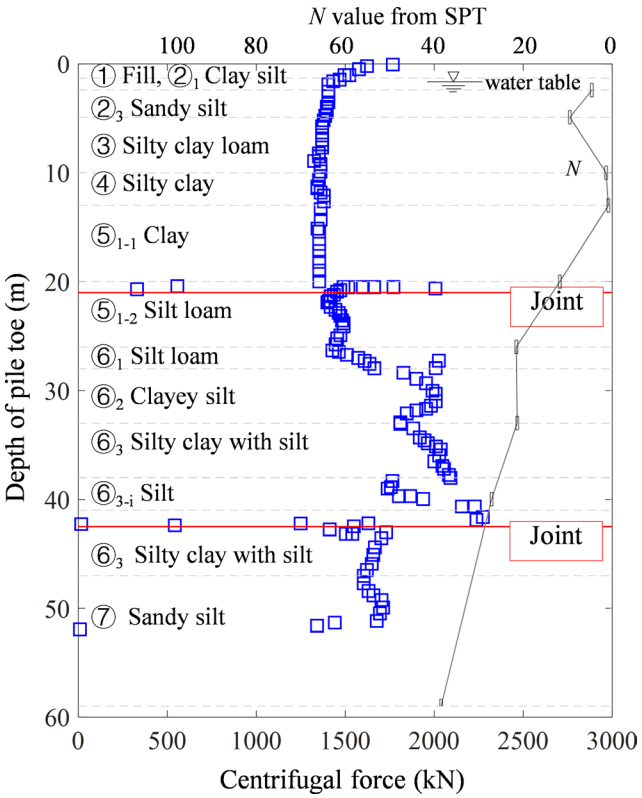

Fig. 7 Vibration driven pile data in Shanghai's soil site

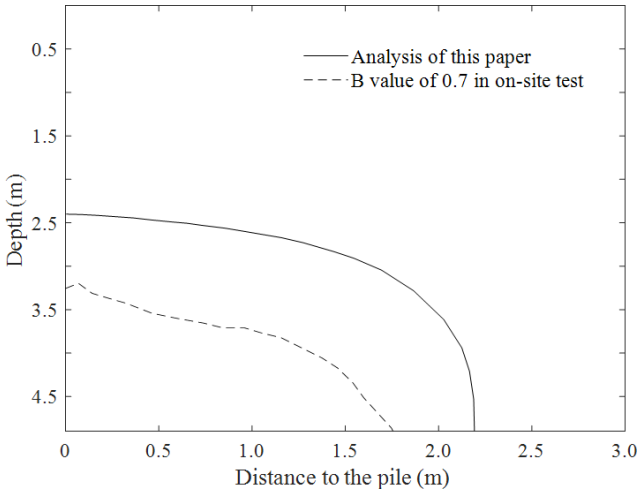

Fig. 8 The comparison of the liquefaction range from calculation and field test in case 1

layer. In contrast, the calculated liquefaction range represents the earliest possible occurrence of liquefaction during the pile driving process, without considering its dissipation over time, and therefore tends to provide an upper-bound estimate. This comparison also indicates that shallow-layer drainage should be considered when interpreting the calculated range for field applications in permeable near-surface soils.

4.2 Case 2

Cheng. [35] conducted a series of vibration liquefaction tests on saturated silt soil using a cross-shaped vibrator and a power frequency inverter at a frequency of 15 Hz. Pore pressure sensors were installed around the vibrating rod to measure the pore water pressure in the surrounding soil during the vibration process. The physical and mechanical properties of the soil layers at the test site are shown in Table 4.

The α–γ relationship for the soil layers can be calculated based on the G / G_{max}–γ and D–γ relations, which were obtained through dynamic triaxial tests, such as α–γ relationship for No. ② silt is as shown in Fig. 9.

Table 4 The physical and mechanical properties of the soil layers at Cheng's test site

Soil layer	Depth / m	Density / kg m^{-3}	Fc / %	Porosity ratio e	Porosity n
① Silty sand	1.5m	1750	12.32	0.55	0.35
② Silt	4.8m	1600	7.80	0.70	0.41
③ Silt	14.8m	1520	6.50	0.79	0.44

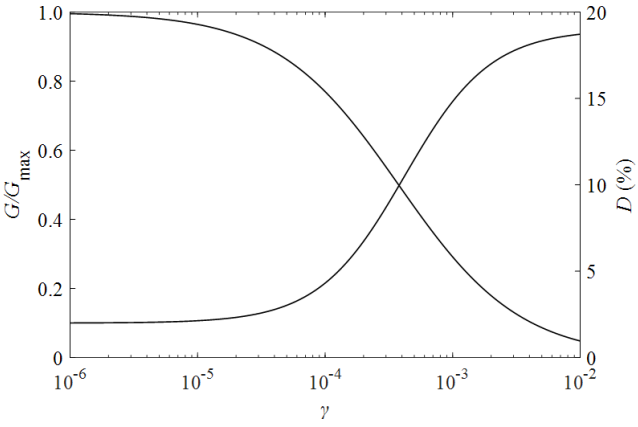

(a)

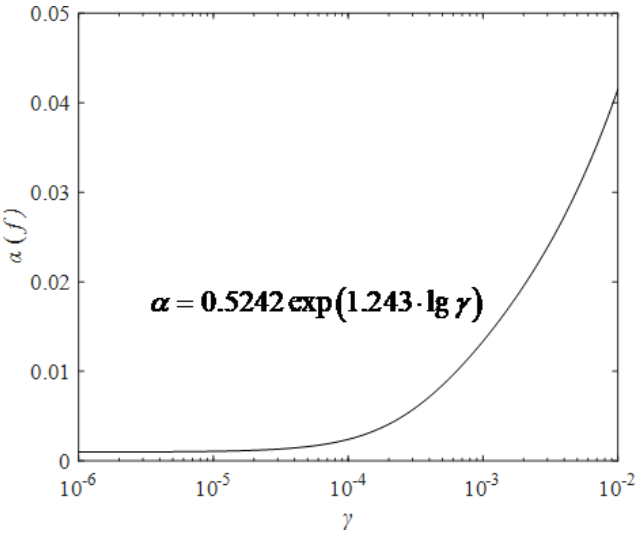

(b)

Fig. 9 The G / G_{max}–γ, D–γ & α~γ relationship for No. ② silt: (a) G / G_{max}–γ and D–γ; (b) α~γ

The energy required for liquefaction at different depths of the soil, i.e. the capacity energy, can be calculated from the SPT data as shown in the Table 5.

During the on-site test, the vibration time was longer than the time threshold t_q, so the shear strain threshold γ_q was set to 0.015%. Based on the parameters of the vibrating hammer, the vibration velocity of the soil adjacent to the pile wall was 0.5 m/s.

According to the method of determining the liquefaction area based on the flowchart presented in the previous section, the liquefaction range of the soil site in Cheng's study was calculated and compared it with the results from on-site testing, as shown in Fig. 10. In Cheng's test, the excess pore pressure ratio, i.e. the ratio of pore water pressure to the average effective stress, exceeding 0.6 was employed to indicate a liquefaction zone, which is used in the analysis. The calculation is in good agreement with the test results.

4.3 Discussion on dissipation effect, uncertainty, and applicability

The proposed framework is intended as a practical engineering tool for early-stage liquefaction risk screening in saturated non-cohesive soils subjected to high-frequency vibratory pile driving. Its principal advantage lies in combining a relatively simple energy-balance concept with strain-dependent dynamic soil behavior and a frequency-sensitive attenuation coefficient. Nevertheless, several limitations should be clarified.

Table 5 The capacity energy for soil liquefaction at different depths

Depth	N	$N_{1,60}$	α	β	$N_{1,60cs}$	N_{ED}
4 m	9	14.1	0.256	0.968	13.9	15.6
5.6 m	14	21.4	0.065	0.973	19.7	50.7
7.1 m	11	16.7	0.065	0.973	16.3	24.4
8.6 m	14	20.8	0.065	0.973	20.3	51.1
10.2 m	11	16.1	0.065	0.973	15.7	21.8

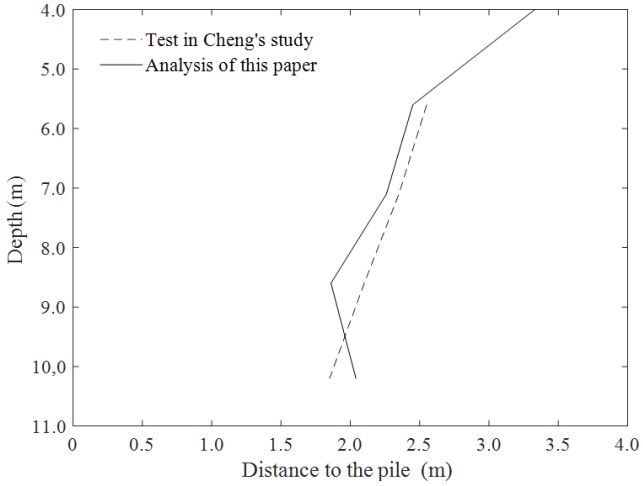

Fig. 10 The comparison of the liquefaction range from calculation and field test in case 2

First, the present model neglects pore-pressure dissipation during vibration. This assumption is more acceptable for short-duration loading or deeper layers with relatively undrained response, but it may lead to conservative predictions in shallow permeable sandy layers where drainage can occur during installation. Therefore, the predicted liquefaction range should be interpreted as an upper-bound or earliest-onset estimate in such layers. For practical use, a simple semi-empirical correction may be introduced by defining an effective transmitted energy as:

$$N_{ED_{eff}} = \eta_d N_{ED}, \tag{15}$$

where $\eta_d \leq 1$ is a drainage-related reduction factor. A lower value of η_d corresponds to stronger dissipation and therefore a smaller predicted liquefaction range. For preliminary engineering sensitivity checks, η_d may be varied within a practical range from 0.7–1.0. A brief sensitivity check shows that decreasing η_d from 1.0 to lower values produces a monotonic reduction in the predicted liquefaction radius, indicating that drainage primarily affects the shallow near-field zone while the overall framework remains stable in its prediction trend.

Second, although the proposed framework is general in formulation, its parameters are not universal constants. In particular, the attenuation coefficient α, the modulus reduction curve $G / G_{\max}$–γ, and the damping curve D–γ are all affected by soil gradation, fines content, relative density, effective confining stress, and saturation conditions. As a result, the method is transferable in structure but requires site-specific calibration for design-level prediction. When such calibration data are unavailable, the framework may still be used for preliminary screening based on representative parameters from similar soil types, but the associated uncertainty should be explicitly acknowledged.

Third, uncertainty in attenuation and fitting parameters may significantly influence the predicted liquefaction extent. Because these parameters are usually obtained from fitted laboratory curves or published empirical relationships, practical applications should include sensitivity checks rather than relying on single deterministic values only. In this study, recommended uncertainty ranges are provided to facilitate such engineering evaluation as shown in Table 6.

5 Conclusions

To evaluate the impact range of vibratory pile driving and ensure pile stability, it is essential to assess and control the

Table 6 Recommended uncertainty ranges for key model parameters in practical applications

Parameter	Source in model	Recommended uncertainty range	Remark
α	Attenuation calibration	± 20%	Sensitive to frequency, soil type, and saturation
G / G_{max}–γ fitting parameters	Dynamic test fitting	± 10% to ± 15%	Depends on data quality and fitting range
D–γ fitting parameters	Dynamic test fitting	±10% to ± 15%	Influences N_{ED} significantly
γ_q	Literature-based threshold	0.015% – 0.020%	Vary with soil fabric and loading history
$N_{1,60CS}$	SPT correction	Site-dependent	Influenced by test variability and fines correction
η_d	Optional drainage correction	0.7 – 1.0	For preliminary shallow-layer sensitivity analysis

liquefaction potential of saturated sandy soils surrounding the pile. This study proposes an energy-based method that compares the vibration energy transmitted during pile driving with the soil's liquefaction energy capacity, enabling effective estimation of potential liquefaction zones. Model-scale experiments reveal that high-frequency vibrations lead to excess pore pressure accumulation and localized instability near the pile, underscoring the need to incorporate frequency effects into the analysis. A frequency-dependent attenuation coefficient is thus introduced to capture the influence of vibration frequency on energy transfer and soil response. Case studies demonstrate the method's effectiveness and its potential for early liquefaction risk assessment. The main conclusions are as follows:

1. By incorporating the shear strain threshold for liquefaction susceptibility, the proposed method enables iterative evaluation of N_{ED} (liquefaction energy demand) and N_{EC} (liquefaction energy capacity). The frequency- and strain-dependent damping ratio replaces the constant damping assumption in traditional models, which is particularly important for high-frequency near-field vibrations.
2. The calculated liquefaction range represents the earliest possible onset of liquefaction during pile driving and does not account for excess pore pressure dissipation over time. As a result, the model may overestimate the actual liquefaction extent, especially in shallow permeable soil layers. For practical applications, this prediction should therefore be interpreted as a conservative upper-bound estimate, and a simple reduction factor or sensitivity check may be introduced when drainage effects are expected to be significant.
3. The proposed framework provides a practical tool for liquefaction risk assessment and construction optimization in saturated non-cohesive soils. By identifying the potential influence zone of vibration-induced liquefaction, it contributes to safer, more rational design and execution of pile foundation systems under undrained conditions in liquefaction-prone areas.

In addition, although the proposed framework is general in structure, its predictive accuracy depends on the quality of the site-specific dynamic soil parameters used for attenuation, modulus reduction, and damping characterization. Future applications should therefore combine the framework with appropriate local calibration and uncertainty evaluation, particularly when extending the method to soils with different gradations, fines contents, and confining stress conditions.

Acknowledgement
This research was funded by the National Natural Science Foundation of China, grant number 42277163.

References

[1] Foglia, A., Kohlmeier, M., Wefer, M. "Physical modeling and numerical analyses of vibro-driven piles with evaluation of their applicability for offshore wind turbine support structures", In: Proceedings of the 17th Nordic Geotechnical Meeting (NGM 2016), Reykjavik, Iceland, 2016, pp. 557–566.

[2] Lamens, P., Askarinejad, A., Sluihsmans, R. W., Feddema, A. "Ground response during offshore pile driving in a sandy slope", Géotechnique, 70(4), pp. 281–291, 2020. https://doi.org/10.1680/jgeot.18.P.023

[3] Matuschek, R., Betke, K. "Measurements of Construction Noise During Pile Driving of Offshore Research Platforms and Wind Farms", In: Proceedings of the NAG/DAGA International Conference on Acoustics, Rotterdam, Netherlands, 2009, pp. 262–265. ISBN 978-1-61839-199-5

[4] Massarsch, K. R., Wersäll, C., Fellenius, B. H. "Vibratory driving of piles and sheet piles – state of practice", Proceedings of the Institution of Civil Engineers – Geotechnical Engineering, 175(1), pp. 31–48, 2022. https://doi.org/10.1680/jgeen.20.00127

[5] Moriyasu, S., Kobayashi, S., Matsumoto, T. "Experimental study on friction fatigue of vibratory driven piles by in situ model tests", Soils and Foundations, 58(4), pp. 853–865, 2018. https://doi.org/10.1016/j.sandf.2018.03.010

[6] Whenham, V., Holeyman, A. "Vibrodriving Prediction Models vs. Experimental Results", In: Proceedings of the Fifth International Conference on Recent Advances in Geotechnical Earthquake Engineering and Soil Dynamics, San Diego, California, 2010, Paper No. 1.17b.

[7] Seed, H. B., Idriss, I. M. "Simplified Procedure for Evaluating Soil Liquefaction Potential", Journal of the Soil Mechanics and Foundations Division, 97(9), pp. 1249–1273, 1971. https://doi.org/10.1061/JSFEAQ.0001662

[8] Seed, R. B., Harder, L. F. "SPT-Based Analysis of Cyclic Pore Pressure Generation and Undrained Residual Strength", In: Proceedings of the H.B. Seed Memorial Symposium, BiTech Publishers, 1990, pp. 351–376.

[9] Dobry, R., Ladd, R. S., Yokel, F. Y., Chung, R. M., Powell, D. "Prediction of Pore Water Pressure Buildup and Liquefaction of Sands During Earthquakes by the Cyclic Strain Method", U.S. Government Printing Office, 1982.

[10] Castro, G. "Liquefaction and Cyclic Mobility of Saturated Sands", Journal of the Geotechnical Engineering Division, 101(6), pp. 551–569, 1975. https://doi.org/10.1061/AJGEB6.0000173

[11] Green, R. A., Mitchell, J. K. "Energy-Based Evaluation and Remediation of Liquefiable Soils", In: Geotechnical Engineering for Transportation Projects,American Society of Civil Engineers, 2004, pp. 1961–1970. ISBN 9780784407448 https://doi.org/10.1061/40744(154)191

[12] Deckner, F. "Vibration transfer process during vibratory sheet pile driving: from source to soil", [online] PhD, Royal Institute of Technology, 2017. Available at: http://www.diva-portal.org/smash/record.jsf?pid=diva2%3A1083184&dswid=1554 [Accessed: 9 Apr 2023]

[13] Viking, K. "Vibro-driveability- a field study of vibratory driven sheet piles in non-cohesive soils", [online] PhD, Royal Institute of Technology, 2002. Available at: http://kth.diva-portal.org/smash/record.jsf?pid=diva2%3A9149&dswid=3065 [Accessed: 9 Apr 2023]

[14] Fardad Amini, P., Noorzad, R. "Energy-based evaluation of liquefaction of fiber-reinforced sand using cyclic triaxial testing", Soil Dynamics and Earthquake Engineering, 104, pp. 45–53, 2018. https://doi.org/10.1016/j.soildyn.2017.09.026

[15] Polito, C., Green, R. A., Dillon, E., Sohn, C. "Effect of load shape on relationship between dissipated energy and residual excess pore pressure generation in cyclic triaxial tests", Canadian Geotechnical Journal, 50(11), pp. 1118–1128, 2013. https://doi.org/10.1139/cgj-2012-0379

[16] Figueroa, J. L., Saada, A. S., Liang, L., Dahisaria, N. M. "Evaluation of Soil Liquefaction by Energy Principles", Journal of Geotechnical Engineering, 120(9), pp. 1554–1569, 1994. https://doi.org/10.1061/(ASCE)0733-9410(1994)120:9(1554)

[17] Sonmezer, Y. B. "Energy-based evaluation of liquefaction potential of uniform sands", Geomechanics and Engineering, 17(2), pp. 145–156, 2019. https://doi.org/10.12989/gae.2019.17.2.145

[18] Bán, Z., Győri, E., Tóth, L., Gráczer, Z., Mahler, A. "Characterization and Liquefaction Hazard Assessment of Two Hungarian Liquefied Sites from the 1956 Dunaharaszti Earthquake", Periodica Polytechnica Civil Engineering, 64(3), pp. 713–721, 2020. https://doi.org/10.3311/PPci.15607

[19] Demir, S. "Numerical Investigation of the Effects of Ground Motion Characteristics on the Seismic Behavior of Liquefiable Soil", Periodica Polytechnica Civil Engineering, 67(1), pp. 24–35, 2023. https://doi.org/10.3311/PPci.19683

[20] Berrabah, F., Guechi, L. "Reliability Analysis of Stone Columns Improved Ground for Mitigation of Liquefaction", Periodica Polytechnica Civil Engineering, 69(4), pp. 1229–1243, 2025. https://doi.org/10.3311/PPci.39716

[21] Massarsch, K. R., Westerberg, E. "The active design concept applied to soil compaction", In: Proceedings of the Bengt B. Broms Symposium in Geotechnical Engineering, World Scientific Pub Co Inc, 1995, pp. 263–276. ISBN 9789810225889

[22] Holeyman, A. E. "An earthquake engineering approach to vibro-compaction", In: Proceedings of the 14th International Conference on Soil Mechanics and Foundation Engineering, CRC Press, 1997, pp. 1603–1608. ISBN 9789054108924

[23] Dowding, C. H. "Construction Vibrations", Prentice-Hall, 1996. ISBN: 9780132991087

[24] Santamarina, J. C., Klein, A., Fam, M. A. "Soils and Waves – Particulate Materials Behavior, Characterization and Process Monitoring", John Wiley & Sons Ltd, 2001. ISBN: 0-471-49058-X

[25] Chen, G., Zhou, Z., Sun, T., Wu, Q., Xu, L., Khoshnevisan, S., Ling, D. "Shear Modulus and Damping Ratio of Sand–Gravel Mixtures Over a Wide Strain Range", Journal of Earthquake Engineering, 23(8), pp. 1407–1440, 2019. https://doi.org/10.1080/13632469.2017.1387200

[26] Hardin, B. O., Drnevich, V. P. "Shear Modulus and Damping in Soils: Design Equations and Curves", Journal of the Soil Mechanics and Foundations Division, 98(7), pp. 667–692, 1972. https://doi.org/10.1061/JSFEAQ.0001760

[27] Robertson, P. K., Wride, C. E. "Evaluating cyclic liquefaction potential using the cone penetration test", Canadian Geotechnical Journal, 35(3), pp. 442–459, 1998. https://doi.org/10.1139/t98-017

[28] Youd, T. L., Idriss, I. M., Andrus R. D., Arango I., Castro, G., …, Stokoe, K. H. "Liquefaction Resistance of Soils: Summary Report from the 1996 NCEER and 1998 NCEER/NSF Workshops on Evaluation of Liquefaction Resistance of Soils", Journal of Geotechnical and Geoenvironmental Engineering, 127(10), pp. 817–833, 2001. https://doi.org/10.1061/(ASCE)1090-0241(2001)127:10(817)

[29] Gujrati, S., Hussain, M., Sachan, A. "Liquefaction Susceptibility of Cohesionless Soils Under Monotonic Compression and Cyclic Simple Shear Loading at Drained/Undrained/Partially Drained Modes", Transportation Infrastructure Geotechnology, 10(3), pp. 391–423, 2023. https://doi.org/10.1007/s40515-022-00226-6

[30] Kishida, T., Tsai, C. C. "Wave velocities depending on shear strain, directionality, and excess pore water pressure from wildlife liquefaction array", Bulletin of Earthquake Engineering, 19(6), pp. 2371–2388, 2021. https://doi.org/10.1007/s10518-021-01074-4

[31] Zhan, J., Chen, J., Wang, W., Li, M. "In situ investigation on pore-water pressure response during vibratory pile driving with high frequency", Acta Geotechnica, 19(5), pp. 2649–2668, 2024. https://doi.org/10.1007/s11440-024-02251-w

[32] Wei, J. "上海地区高频免共振钢管桩贯入过程桩土响应与承载特性研究" (Pile-soil response during penetration and bearing characteristics of high-frequency resonance-free steel pipe pile in Shanghai), PhD, Tongji University, 2022. (in Chinese)

[33] El Takch, A., Sadrekarimi, A., El Naggar, H. "Cyclic resistance and liquefaction behavior of silt and sandy silt soils", Soil Dynamics and Earthquake Engineering, 83, pp. 98–109, 2016. https://doi.org/10.1016/j.soildyn.2016.01.004

[34] Saeid, A. L., Mahmoud, Y., Arya, A. L. "A study on the liquefaction risk in seismic design of foundations", Geomechanics and Engineering, 11(6), pp. 805–820, 2016. https://doi.org/10.12989/gae.2016.11.6.805

[35] Cheng, Y. "振杆密实法加固可液化地基理论与应用研究" (Research on the theory and application of vibrating rod compaction method for reinforcing liquefiable foundations), PhD, Southeast University, 2013. (in Chinese)